Aerospace Science and Technology 29 (2013) 386–393

Contents lists available at SciVerse ScienceDirect

Aerospace Science and Technology

www.elsevier.com/locate/aescte

# Thermally induced vibrations of flexible beams using Absolute Nodal Coordinate Formulation

Zhenxing Shen, Qiang Tian, Xiaoning Liu, Gengkai Hu *

*Key Laboratory of Dynamics and Control of Flight Vehicle, Ministry of Education, School of Aerospace Engineering, Beijing Institute of Technology, Beijing 100081, China*

ARTICLE INFO

*Article history:*
Received 12 April 2012
Received in revised form 23 April 2013
Accepted 24 April 2013
Available online 2 May 2013

*Keywords:*
Thermally induced vibrations
Thermal flutter
Thin-walled tube
Absolute Nodal Coordinate Formulation (ANCF)
Finite element method

ABSTRACT

A coupled thermal–structural analysis based on the Euler–Bernoulli beam model is conducted within a framework of Absolute Nodal Coordinate Formulation. The absorbed heat flux on the beam surface depends on actual deformation and motion of the beam, therefore the coupled transient heat conduction equation and structural dynamics equation are established and solved interactively by the generalized-$\alpha$ scheme. Thermally induced vibrations for a thin-walled tubular boom subjected to a sudden heating in order to simulate spacecraft's exit from eclipse, and structure dynamics of a rotating flexible manipulator in a thermal environment are examined in details. With the coupled thermal–structural analysis, the thermal flutter can be well predicted for a cantilever beam moving from eclipse with large incident angles of solar radiation, and the proposed model is also able to characterize the coupled thermal–structural dynamics when a flexible beam is subjected to a large rotation. The developed model can be served as a basic unit for analyzing thermal–mechanical coupling response of large flexible space structures based on the Absolute Nodal Coordinate Formulation.



## 1. Introduction

The thermal environment in earth orbit is around 100 °C on sunlight surface, and as low as −100 °C on shadow side [17]. When a spacecraft enters into or exits from eclipse, thermally induced oscillations may take place due to a sudden change in heat flux of solar radiation. This rapid change in the thermal loading produces a thermal moment across spacecraft appendage, this thermal moment coupled in turn with structural deformation may lead to unstable oscillation or thermal flutter of the structure [21,23,25]. Thermally induced vibrations of flexible space structures have been observed during the flight of the OGO-IV spacecraft in the 1960s [21], and a pointing "jitter" was also found due to thermally induced bending vibrations of the solar arrays when the Hubble Space Telescope was moving from shadow to sunlight [7].

These thermally induced vibrations were first addressed by Boley, and he established an uncoupled theory and identified the ratio between the thermal response time and the structural response time as a key parameter to characterize the occurrence of these thermally induced vibrations [3]. Later, Thornton and Kim proposed a coupled thermal–structural analysis to demonstrate unstable thermally induced vibration (thermal flutter) of a spacecraft boom [22]. Since then, these coupled thermal–structural vibrations are examined by different analytical and computational methods [14,24], and experiments in the earth environment have also been conducted to validate simulations [6,15].

Large space structures are usually deployed in orbit from a number of building units connected in a flexible way, there is a great demand for efficient computational algorithms to simulate their thermal and mechanical dynamic performances. The Absolute Nodal Coordinate Formulation (ANCF) developed by Shabana [19] can accurately model a deformable body with large deformation and motion, and it is applied to characterize the deployment dynamics for antennas [16,18]. During the deployment process, the building units will undergo large motion and rotation in addition to deformation, therefore it is necessary to develop an efficient computation method based on ANCF to analyze the coupled thermal–structural behavior of such structure. The purpose of this paper is to examine thermally induced bending vibrations for a thin-walled tubular boom within the framework of ANCF, coupled thermal–structural dynamics equations will be derived. The developed model will be applied to examine the thermal effect including thermal flutter for a spacecraft boom with or without large rotation.

* Corresponding author.
*E-mail address:* hugeng@bit.edu.cn (G. Hu).

1270-9638/$ – see front matter 
http://dx.doi.org/10.1016/j.ast.2013.04.009

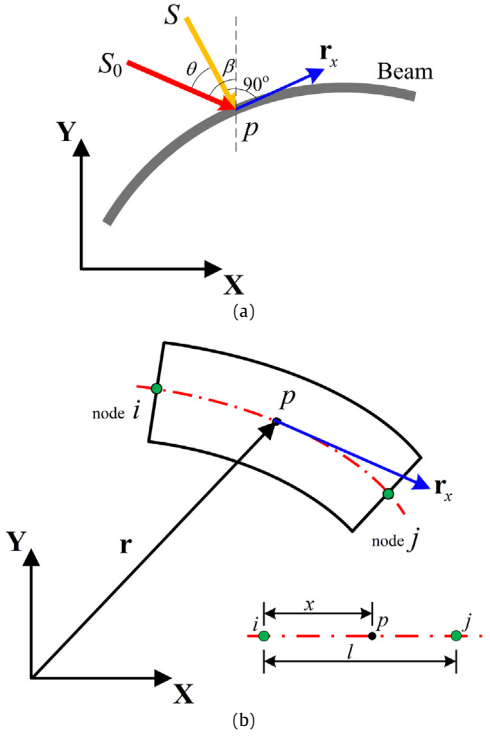


**Fig. 1.** (a) Heat flux of coupled thermal–structural analysis. (b) Euler–Bernoulli beam element in ANCF.

## 2. Coupled thermal–structural formulation

### 2.1. Structure dynamics with thermal effect

Consider a planar Euler–Bernoulli beam element in an actual configuration, which is exposed to a heat flux $S_0$ with an angle $\theta$ to the normal of the neutral axis of the beam at a point $p$, which is shown in Fig. 1a. Since the deformation of the beam will alter absorbed heat flux $S$, therefore this will lead to a coupled thermal–structural problem. To this end, we will first formulate the structure dynamics problem with thermal effect. In this case, the thermal effect is considered by introducing an average temperature $\bar{T}$ over the beam cross-section, and a thermal moment $M_T$, which will be determined iteratively by the subsequent thermal analysis explained in the next section.

As shown in Fig. 1b, a position vector $\mathbf{r}$ of an arbitrary point $p$ on the beam in ANCF is given by [2]

$$\mathbf{r} = \mathbf{N}\mathbf{e}, \tag{1}$$

where $\mathbf{N}$ is the shape function of the Euler–Bernoulli beam element, written as

$$\mathbf{N} = \begin{bmatrix} n_1 & 0 & n_2 l & 0 & n_3 & 0 & n_4 l & 0 \\ 0 & n_1 & 0 & n_2 l & 0 & n_3 & 0 & n_4 l \end{bmatrix}, \tag{2}$$

and the components $n_i$ $(i = 1, 2, 3, 4)$ are given by

$$n_1 = 1 - 3\xi^2 + 2\xi^3, \qquad n_2 = \xi - 2\xi^2 + \xi^3,$$
$$n_3 = 3\xi^2 - 2\xi^3, \qquad n_4 = -\xi^2 + \xi^3, \tag{3}$$

where $\xi = x/l$, $l$ is the element length, and $x$ is the element coordinate.

In Eq. (1), the vector of element nodal coordinates $\mathbf{e}$ is defined as

$$\mathbf{e} = \left[ \mathbf{r}^{\mathrm{T}}|_{x=0}, \quad \mathbf{r}_x^{\mathrm{T}}|_{x=0}, \quad \mathbf{r}^{\mathrm{T}}|_{x=l}, \quad \mathbf{r}_x^{\mathrm{T}}|_{x=l} \right]^{\mathrm{T}}, \tag{4}$$

where $\mathbf{r}^{\mathrm{T}}|_{x=0}$ and $\mathbf{r}^{\mathrm{T}}|_{x=l}$ are the global displacements of the nodes; $\mathbf{r}_x^{\mathrm{T}}|_{x=0}$ and $\mathbf{r}_x^{\mathrm{T}}|_{x=l}$ are the global slopes at the nodes, with the definition $\mathbf{r}_x = \partial \mathbf{r}/\partial x$.

The kinetic energy of the beam element is defined as follows:

$$T = \frac{1}{2}\int_V \rho \dot{\mathbf{r}}^{\mathrm{T}}\dot{\mathbf{r}}\,\mathrm{d}V = \frac{1}{2}\dot{\mathbf{e}}^{\mathrm{T}}\left(\int_V \rho \mathbf{N}^{\mathrm{T}}\mathbf{N}\,\mathrm{d}V\right)\dot{\mathbf{e}} = \frac{1}{2}\dot{\mathbf{e}}^{\mathrm{T}}\mathbf{M}\dot{\mathbf{e}}, \tag{5}$$

where $\mathbf{M}$ is a constant mass matrix and is expressed as

$$\mathbf{M} = \int_V \rho \mathbf{N}^{\mathrm{T}}\mathbf{N}\,\mathrm{d}V, \tag{6}$$

in which $V$ is the element volume, $\rho$ is the mass density.

For the Euler–Bernoulli beam, the longitudinal strain energy of the element including thermal effect can be written as [4]

$$U_l = \frac{1}{2}\int_0^l EA\left(\varepsilon_l - \varepsilon_T^l\right)^2 \mathrm{d}x, \tag{7}$$

where $E$ is the Young modulus, $A$ is the cross-sectional area of the beam, $\varepsilon_l$ is the longitudinal strain, and $\varepsilon_T^l$ is the longitudinal thermal strain. Here, the thermally induced longitudinal strain $\varepsilon_T^l$ is written as

$$\varepsilon_T^l = \alpha_T(\bar{T} - T_0), \tag{8}$$

where $\alpha_T$ is the coefficient of thermal expansion, $\bar{T}$ is the average temperature over the cross-section, and $T_0$ is a reference temperature.

The longitudinal elastic force $\mathbf{Q}_l$ is defined as [2]

$$\mathbf{Q}_l = \left(\frac{\partial U_l}{\partial \mathbf{e}}\right)^{\mathrm{T}} = \mathbf{K}_l\mathbf{e}, \tag{9}$$

where the longitudinal stiffness matrix $\mathbf{K}_l$ can be written as

$$\mathbf{K}_l = \int_0^l EA\left(\varepsilon_l - \varepsilon_T^l\right)\mathbf{N}_l\,\mathrm{d}x = \frac{1}{2}EA\int_0^l \left(\mathbf{e}^{\mathrm{T}}\mathbf{N}_l\mathbf{e} - 1 - 2\varepsilon_T^l\right)\mathbf{N}_l\,\mathrm{d}x, \tag{10}$$

and $\mathbf{N}_l$ is written as

$$\mathbf{N}_l = \frac{1}{l^2}\mathbf{N}_\xi^{\mathrm{T}}\mathbf{N}_\xi, \tag{11}$$

where $\mathbf{N}_\xi$ is the derivative of the shape function $\mathbf{N}$ with respect to $\xi$.

The transverse thermal strain $\varepsilon_T^t$ is usually small, therefore the high order term $(\varepsilon_T^t)^2$ will be neglected in the following analysis. Thus, the transverse strain energy of the beam element with thermal effect is given by

$$\begin{aligned} U_t &= \frac{1}{2}\int_V E\left(\varepsilon_t - \varepsilon_T^t\right)^2 \mathrm{d}V \approx \frac{1}{2}\int_V E\varepsilon_t^2\,\mathrm{d}V - \int_V E\varepsilon_t.\varepsilon_T^t\,\mathrm{d}V \\ &= \frac{1}{2}\int_0^l EI\left(K|\mathbf{r}_x|\right)^2\mathrm{d}x - \int_0^l M_T K|\mathbf{r}_x|\,\mathrm{d}x, \end{aligned} \tag{12}$$

where $\varepsilon_t$ is the transverse strain, $I$ is the cross-sectional moment of inertia, $K$ is the material curvature and defined by [10]

$$K = \frac{|\mathbf{r}_x \times \mathbf{r}_{xx}|}{|\mathbf{r}_x|^2}. \tag{13}$$

In Eq. (12), the thermal moment $M_T$ is defined as [4]

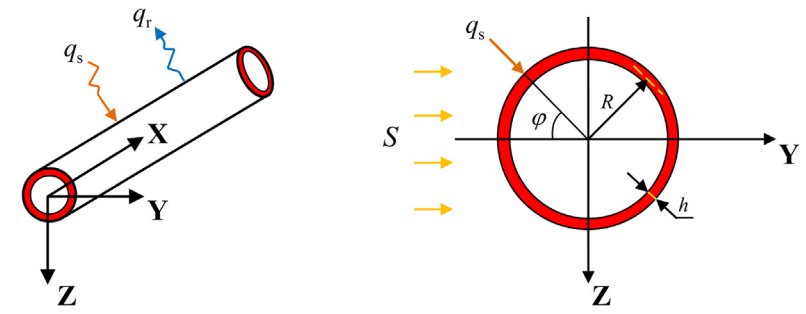


(a) Thin-walled tube and heat flux (b) Thin-walled tube cross-section

**Fig. 2.** Thermal model of a boom.

$$M_T = \int_A E(\alpha_T \Delta T) Y \, \mathrm{d}A, \tag{14}$$

where $\Delta T$ is the temperature difference along the beam's cross-section.

The transverse elastic force $\mathbf{Q}_t$ is then obtained as

$$\mathbf{Q}_t = \left(\frac{\partial U_t}{\partial \mathbf{e}}\right)^{\mathrm{T}} = \mathbf{K}_t(\mathbf{e})\mathbf{e}, \tag{15}$$

where $\mathbf{K}_t(\mathbf{e})$ is the transverse stiffness matrix, and it is written as

$$\mathbf{K}_t(\mathbf{e}) = \frac{1}{2} EI \mathbf{K}_1 - M_T \mathbf{K}_2, \tag{16}$$

where

$$\mathbf{K}_1 = \int_0^l 4\mathbf{N}_t \frac{(\mathbf{e}^{\mathrm{T}}\mathbf{N}_t\mathbf{e})}{(\mathbf{e}^{\mathrm{T}}\mathbf{N}_f\mathbf{e})} - 2\mathbf{N}_f \frac{(\mathbf{e}^{\mathrm{T}}\mathbf{N}_t\mathbf{e})^2}{(\mathbf{e}^{\mathrm{T}}\mathbf{N}_f\mathbf{e})^2} \, \mathrm{d}x, \tag{17}$$

$$\mathbf{K}_2 = \int_0^l 2\mathbf{N}_t (\mathbf{e}^{\mathrm{T}}\mathbf{N}_f\mathbf{e})^{-0.5} - \mathbf{N}_f (\mathbf{e}^{\mathrm{T}}\mathbf{N}_t\mathbf{e})(\mathbf{e}^{\mathrm{T}}\mathbf{N}_f\mathbf{e})^{-1.5} \, \mathrm{d}x, \tag{18}$$

and

$$\mathbf{N}_t = \frac{1}{2}(\bar{\mathbf{N}}_t + \bar{\mathbf{N}}_t^{\mathrm{T}}), \qquad \bar{\mathbf{N}}_t = \frac{1}{l^3}\mathbf{N}_\xi^{\mathrm{T}} \begin{bmatrix} 0 & -1 \\ 1 & 0 \end{bmatrix} \mathbf{N}_{\xi\xi},$$

$$\mathbf{N}_f = \frac{1}{l^2}\mathbf{N}_\xi^{\mathrm{T}}\mathbf{N}_\xi. \tag{19}$$

According to Lagrange's equation [20], the equation of motion for the beam element is then derived as in a matrix form

$$\mathbf{M}\ddot{\mathbf{e}} + \mathbf{Q}_e + \mathbf{Q}_{\mathrm{ext}} = \mathbf{0}, \tag{20}$$

where $\mathbf{Q}_{\mathrm{ext}}$ is the generalized external forces, and $\mathbf{Q}_e$ is the elastic force and given by

$$\mathbf{Q}_e = \mathbf{Q}_l + \mathbf{Q}_t. \tag{21}$$

Finally, Eq. (20) is solved iteratively by the generalized-$\alpha$ method [1,5] when the temperature over the beam cross-section is known in each incremental time step.

### 2.2. Thermal analysis

In this section, a spacecraft boom [21] is considered in order to obtain the temperature field necessary for solving the structural dynamics problem explained in Section 2.1. The boom is a thin-walled tubular beam, which is shown in Fig. 2. In Fig. 2a, $q_s$ is the absorbed heat flux of the thin-walled tube, and it is related to the element surface absorptivity; $q_r$ is the outward radiation heat flux from the exterior tube surface. In Fig. 2b, $S$ denotes the absorbed heat flux from the solar radiation, which is perpendicular to the global slope of the tube $\mathbf{r}_x$, and it can be determined by the current configuration of the beam, as illustrated in Fig. 1a. In the coupled thermal–structural analysis, the heat flux $q_s$ is related to the structural deformation by

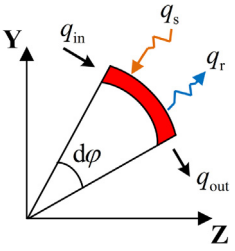


**Fig. 3.** A differential tube element.

$$q_s = \alpha_s S = \alpha_s S_0 \cos\theta, \tag{22}$$

where $\alpha_s$ is the surface absorptivity of the tube, $S_0$ is the value of the solar radiation, and $\theta$ is the intersection angle between the solar radiation heat flux $S_0$ and the absorbed heat flux $S$ (see Fig. 1a). $\theta$ is derived from the global slope $\mathbf{r}_x$ and the incident angle $\beta$ of the solar flux, once the deformation of the beam is evaluated.

For the thermal analysis of the thin-walled tube, the following assumptions are made [12,21]: the temperature gradient is neglected along the wall thickness due to small wall thickness $h$; the heat convection is also neglected because of high vacuum and low pressure space environment; the radiation heat exchange amongst internal surfaces is neglected for the thin-walled tube, and finally thermal properties of the thin-walled tube are assumed to be temperature independent.

To proceed, a differential tube element in circumference is adopted to establish the heat transfer equation at each cross-section, as shown in Fig. 3. $q_{in}$ and $q_{out}$ are the heat flux conducted into and heat flux conducted out of the tube element, respectively. According to the first law of thermodynamics, the thermal governing equation is derived as

$$\frac{\partial T}{\partial t} - \frac{k}{\rho c R^2}\frac{\partial^2 T}{\partial \varphi^2} + \frac{\sigma\varepsilon}{\rho c h} T^4 = \frac{\alpha_s S}{\rho c h}\delta\cos\varphi, \tag{23}$$

where $k$ is the thermal conductivity, $R$ is the radius of the tube, and $c$ is the specific heat, $\sigma$ is the Stefan–Boltzmann constant, and $\varepsilon$ is the emissivity of the external tube surface. The parameter $\delta$ is used to define the external surface of the tube in which suffers the solar radiation:

$$\delta = \begin{cases} 1, & -\pi/2 < \varphi < \pi/2, \\ 0, & \pi/2 < \varphi < 3\pi/2. \end{cases} \tag{24}$$

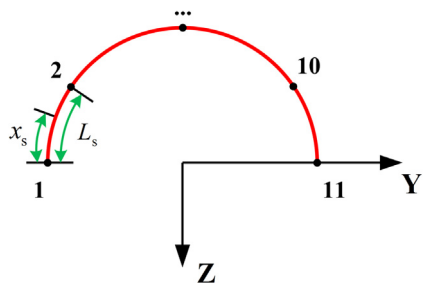


**Fig. 4.** Finite element discretization of the tube semi-cross-section.

On the right-hand side of Eq. (23), $S$ is the value of the heat flux projected normally to the external surface of the tube, and it varies along the tube length due to the beam deformation. So the temperature $T(X,\varphi,t)$ depends on $X$ and $\varphi$. Therefore, Eq. (23) describes a nonlinear transient heat transfer problem, and it can be solved by a finite element method after discretization of the structure [11],

$$\mathbf{C}\dot{\mathbf{T}} + (\mathbf{K}_c + \mathbf{K}_r)\mathbf{T} = \mathbf{R}_q, \tag{25}$$

where $\dot{\mathbf{T}} = \partial\mathbf{T}/\partial t$, and $\mathbf{T}$ is the unknown nodal temperature, the coefficient $\mathbf{C}$ is the element capacitance matrix, the coefficients $\mathbf{K}_c$ and $\mathbf{K}_r$ are element conductance matrices related to conduction and radiation, respectively. The vector $\mathbf{R}_q$ is the heat loading vector due to surface radiant heating, and it is related to the structural deformation. Due to the symmetry, the finite element discretization for the tube semi-cross-section is shown in Fig. 4, one-dimensional two node element is used. In a local element coordinate, the element shape functions are given by

$$N_{T,1}(x_s) = 1 - \frac{x_s}{L_s}, \qquad N_{T,2}(x_s) = \frac{x_s}{L_s}, \tag{26}$$

where $x_s$ is the element local coordinate along the circle, and $L_s$ is an element arc-length. Therefore, the coefficients in Eq. (25) for a two node element are obtained by [11]

$$\begin{aligned}
\mathbf{C} &= \frac{\rho c h L_s}{6}\begin{bmatrix} 2 & 1 \\ 1 & 2 \end{bmatrix}, \qquad \mathbf{K}_c = \frac{kh}{L_s}\begin{bmatrix} 1 & -1 \\ -1 & 1 \end{bmatrix}, \\
\mathbf{R}_q &= \frac{q_s L_s}{2}\begin{bmatrix} 1 \\ 1 \end{bmatrix},
\end{aligned} \tag{27}$$

$$\begin{aligned}
\mathbf{K}_r = {} & \frac{\sigma\varepsilon L_s}{60} \\
& \times \begin{bmatrix} 10T_1^3 + 6T_1^2T_2 + 3T_1T_2^2 + T_2^3 & 2T_1^3 + 3T_1^2T_2 + 3T_1T_2^2 + 2T_2^3 \\ 2T_1^3 + 3T_1^2T_2 + 3T_1T_2^2 + 2T_2^3 & T_1^3 + 3T_1^2T_2 + 6T_1T_2^2 + 10T_2^3 \end{bmatrix},
\end{aligned} \tag{28}$$

where $T_1$ and $T_2$ are the nodal temperatures.

The coupled thermal–structural analysis is performed by solving interactively the nonlinear equations (25) and (20) in each time step.

### 2.3. Validation

A simply supported rectangular beam of length $L$ and height $h_r$ under a constant heat input $Q$ on the top surface with the bottom surface insulated is examined to validate the proposed model based on ANCF, as shown in Fig. 5. Only heat conduction is considered in this thermal analysis. The thermal–structural property and the temperature field of the beam are given in Ref. [4].

The non-dimensional mid-span transverse displacement $V = \pi^4 k v/(192 Q \alpha_T L^2)$ is evaluated by the proposed method and it is also compared with Boley's result [4]. The comparison results are

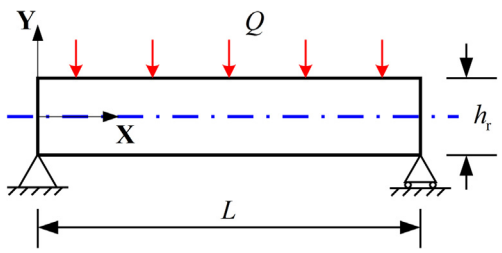


**Fig. 5.** Rectangle beam subjected to surface heating.

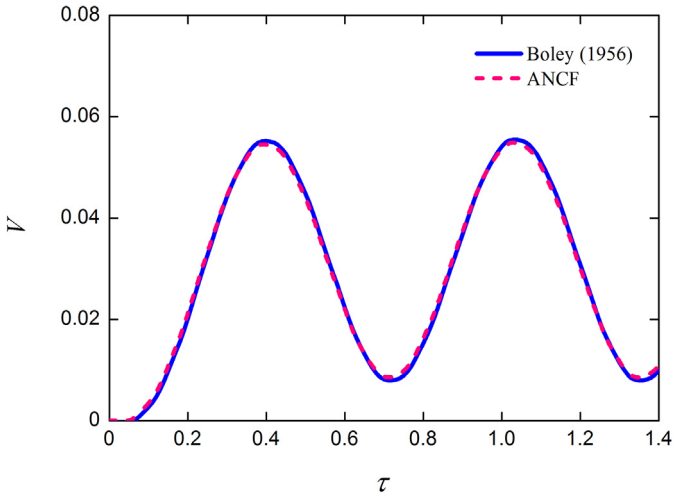


**Fig. 6.** Non-dimensional mid-span transverse displacement as a function of time.

shown in Fig. 6, where $\tau = \kappa_T t/h_r^2$ is a non-dimensional time parameter, $\kappa_T$ is the thermal diffusivity, $t$ is the time, and $v$ is the transverse displacement. A good agreement between two methods is found, so in the following the proposed model in Section 2 will be used to examine thermally induced vibrations of a spacecraft boom with or without a large rotation.

## 3. Numerical results and discussions

### 3.1. A cantilevered thin-walled tube

A cantilevered thin-walled tube with a tip mass rest at initial horizon position is considered by the proposed method, which is shown in Fig. 7. The solar heat flux $S_0$, approximately 1350 W/m$^2$, is suddenly imposed on the tube with an incident angle $\beta$. The black body radiating temperature of the space environment is considered as 0 K in the thermal analysis, and the initial temperature $T_0$ is set to be 290 K for the thin-walled tube. The other parameters are listed in Table 1 [13]. The makeup of the tip mass is also shown in Fig. 7, which is a viscous-fluid damper [25]. Thus, in the structure, the damping force is only supplied by the tip mass and the damping due to material is neglected. Therefore the damping force is included in the generalized external forces of the tip element as

$$\mathbf{Q}_{\text{ext}} = 2\zeta\omega_0\left(m\mathbf{N}_{\xi=1}^{\mathrm{T}}\mathbf{N}_{\xi=1}\right)\dot{\mathbf{e}}, \tag{29}$$

where $\zeta$ is the damping ratio, and $\omega_0$ is the first mode natural frequency [21]. If the damping effect of material is considered, the formulation given in Ref. [9] should be used.

According to Thornton and Foster [21], the thermal flutter takes place if the non-dimensional parameters satisfy the following condition:

$$\eta > \frac{2\zeta}{\lambda} + 4\zeta^2 + 2\zeta\lambda. \tag{30}$$

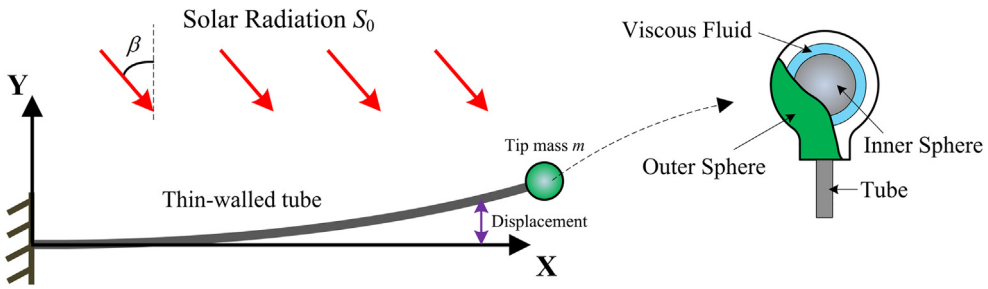


**Fig. 7.** The structure model of a spacecraft boom.

**Table 1**
Properties of the thin-walled tube.

| $\rho$ (kg/m$^3$) | $h$ (mm) | $R$ (mm) | $L$ (m) | $E$ (GPa) | $m$ (kg) | $c$ (J/(kg k)) | $k$ (W/(m K)) | $\alpha_T$ (1/K) | $\alpha_s$ | $\varepsilon$ |
|---|---|---|---|---|---|---|---|---|---|---|
| 8026 | 0.203 | 9.53 | 7.5 | 152.18 | 1.5 | 502 | 16.6 | $1.69 \times 10^{-5}$ | 0.5 | 0.13 |

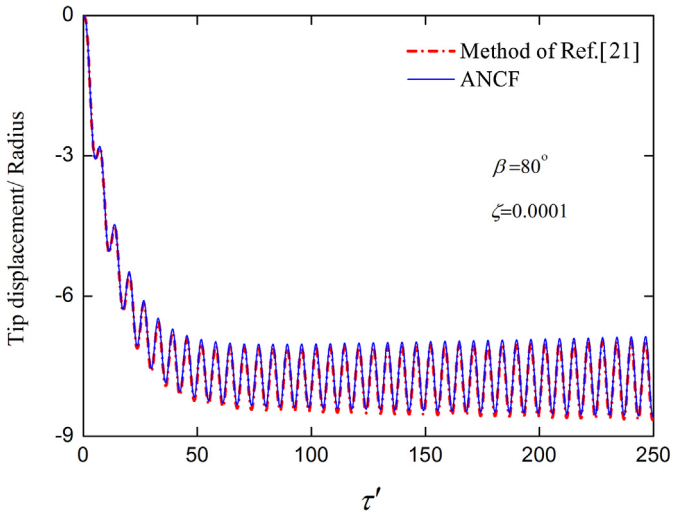


**Fig. 8.** Tip displacement for the coupled unstable response.

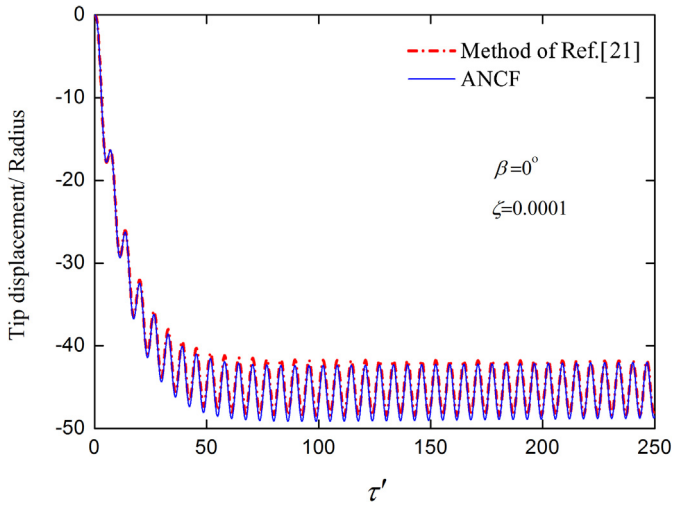


**Fig. 9.** Tip displacement for the coupled stable response.

These non-dimensional parameters are defined as

$$\eta = \frac{3}{4}\frac{L}{2R}\alpha_T T^* \sin\theta, \qquad \lambda = \frac{1}{\omega_0 \gamma}, \tag{31}$$

where

$$\frac{1}{\gamma} = \frac{k}{\rho c R^2} + \frac{4\sigma\varepsilon}{\rho c h}\left(\frac{\alpha_s S_0 \cos\theta}{\pi\sigma\varepsilon}\right)^{\frac{3}{4}}, \qquad T^* = \frac{1}{2}\frac{\alpha_s S_0}{\rho c h}\gamma. \tag{32}$$

Fig. 8 shows the thermally induced vibration of the tip mass on the boom for $\beta = 80°$ and $\zeta = 0.0001$ where thermal flutter takes place according to Eq. (30), the non-dimensional time parameter is defined as $\tau' = \omega_0 t$, the predicted vibration response indeed becomes unstable in this case. The predicted vibration response is also compared with the analytical result given by Thornton and Foster [21], once again it is showed that the prediction based on the ANCF agrees well with that based on the analytical solution for the coupled thermal–structural analysis. Additionally, Fig. 9 shows the predicted vibration response for $\beta = 0°$ and $\zeta = 0.0001$ where the response is stable by condition (30). Again the proposed model based on the ANCF can well predict this coupled thermal–structural analysis and agrees well with the analytical solution. It can be found that the structural stability is related to the solar incident angle $\beta$, and when the solar incident angle is decreased, the tip displacement is increased because of the increase of the absorbed heat flux $S$ which leads to the increase of thermal moment $M_T$ in the thin-walled tube.

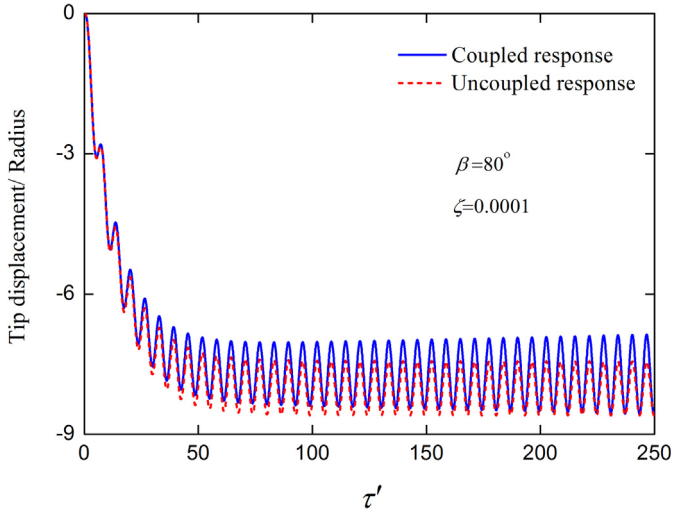


**Fig. 10.** Tip displacements for coupled and uncoupled analysis.

Fig. 10 shows the predicted responses of the boom with the coupled and uncoupled thermal–structural models based on the ANCF, it is seen that the uncoupled thermal–structural model predicts always stable response even in the case where thermal flutter occurs. In the uncoupled thermal–structural analysis, the absorbed heat flux is independent of the structural deformation, the

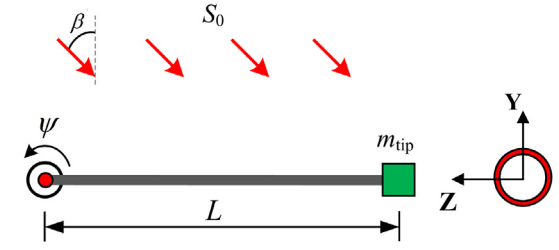


**Fig. 11.** A rotating manipulator under thermal radiation.

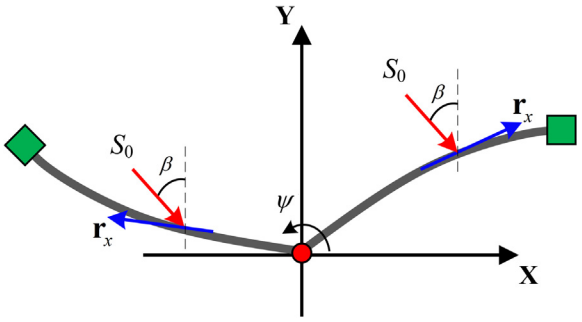


**Fig. 12.** Deformation of a rotating manipulator at different instants.

coupling between thermal and structural response can't be taken into account.

### 3.2. A rotating flexible manipulator

To further demonstrate capacity of the proposed model, a rotating flexible manipulator in a thermal environment will be examined. The manipulator drives a 3 m long thin-walled tube with a tip mass 1.5 kg to rotate at a speed $\dot{\psi}(t)$ in the space environment, which is shown in Fig. 11, and the other properties of the thin-walled tube are the same as those given in the first example. When the flexible manipulator starts to rotate and deform (see Fig. 12), there may exist a situation where one part of the manipulator will shadow the another if the beam is too flexible. This situation is not considered in our analysis by assuming that the transverse deflection is relatively small compared to the length of the manipulator. The angle of rotation is assumed to be the following form [8]:

$$\psi(t) = \begin{cases} \frac{\Omega}{T}[\frac{t^2}{2} + (\frac{T}{2\pi})^2(\cos\frac{2\pi t}{T} - 1)], & t < T, \\ \Omega(t - \frac{T}{2}), & t \geqslant T, \end{cases} \tag{33}$$

and $T = 15$ s; two values of $\Omega = 2$ rad/s, 4 rad/s are considered.

Firstly, the influence of the number of elements is examined, Fig. 13 shows that the computation with 6 elements is enough to give a steady prediction, and it will be used in the following analysis. The angle between the solar radiation heat flux vector $S_0$ and the tangent vector of the neutral axis of the deflected beam $\mathbf{r}_x$ changes with time due to the deformation and rotation of the tube. Fig. 14 shows the normalized tip deflections as a function of normalized time for the angular velocities $\Omega = 4$ rad/s and 2 rad/s with two initial incident angles $\beta = 0°$ and 80°, respectively. It is shown that the thermal effect may have an important influence on dynamic response of the manipulator, which is due to the fact that the thermal moment induces a bending deformation for the thin-walled tube. The initial incident angle has little influence on the structural dynamics since the tube is rotated in the space, as expected. As the angular velocity is decreased, the thermal radiation effect becomes relatively pronounced because of the reduction of the deflection due to inertia effect, as shown in Fig. 14.

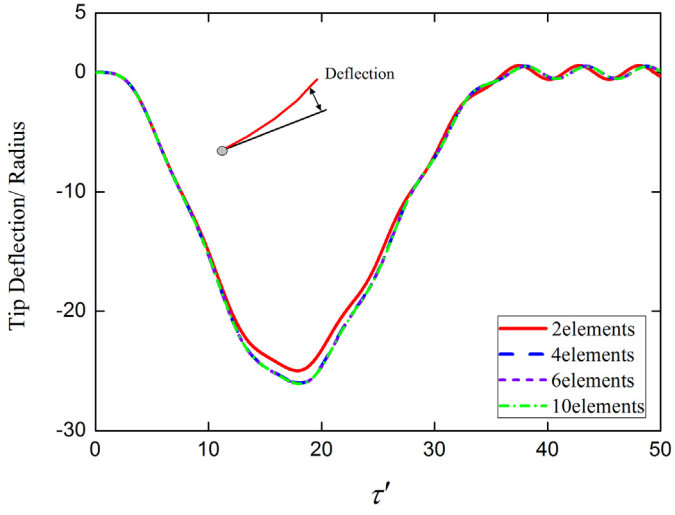


**Fig. 13.** Tip deflection of a rotating manipulator computed with different elements without thermal load ($\Omega = 4$ rad/s).

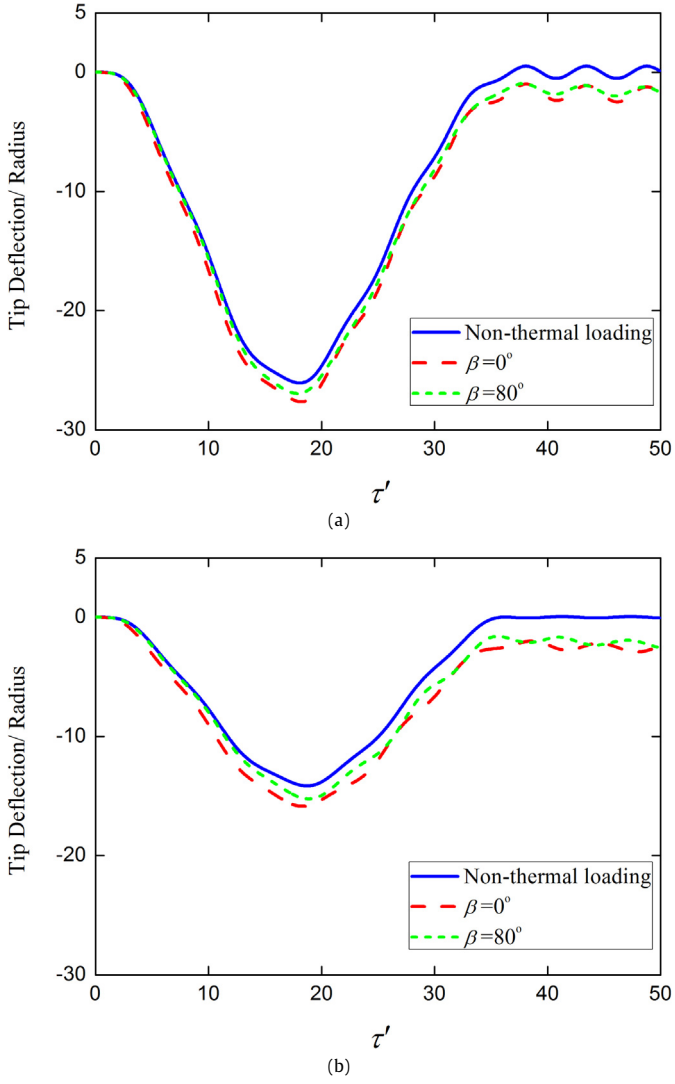


**Fig. 14.** Tip deflection of the rotating manipulator. (a) $\Omega = 4$ rad/s. (b) $\Omega = 2$ rad/s.

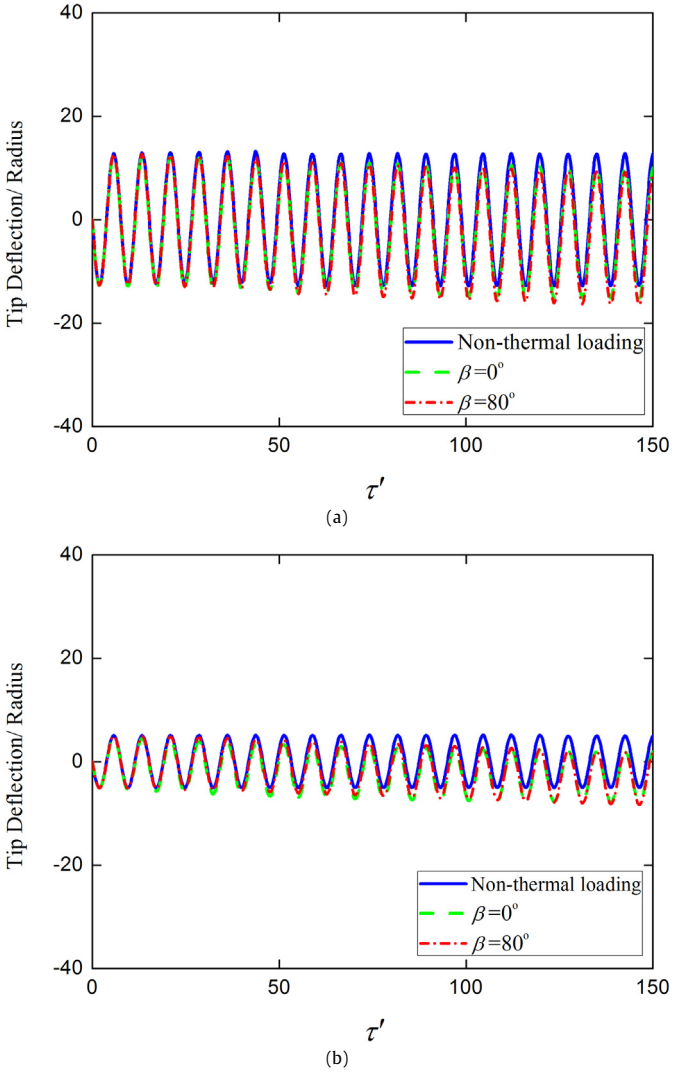


**Fig. 15.** Tip deflection of the rotation manipulator. (a) $\Omega = 0.25$ rad/s. (b) $\Omega = 0.1$ rad/s.

Another motor motion of 1.0 rad at a speed of $\dot{\psi}(t)$ is also examined, and the angle of rotation is written in the following form:

$$\psi(t) = \begin{cases} \sin(\Omega t), & t < T, \\ 1, & t \geqslant T, \end{cases} \tag{34}$$

and $T = \pi/2\Omega$ with $\Omega = 0.1$ rad/s, 0.25 rad/s, respectively.

The manipulator drives also a 3 m long thin-walled tube, but the tip mass is now 0.15 kg. The other properties of the tube remain the same as in Table 1.

In this case, only the top surface of the tube is suffered solar radiation during the motion since the tube is fixed after a motion of 1.0 rad. Different initial incident angles and the responses without thermal loading are also examined and illustrated for comparison. Again, the effect of the initial incident angle is not significant due to the rotation of the tube, and for small angular velocity, the thermal effect is relatively more pronounced due to the small deflection amplitude caused by low angular velocity, these are shown in Fig. 15. From these results, it is seen that considering the thermal effect is necessary to give an accurate prediction on the manipulator dynamics in the space environment.

## 4. Summary and conclusions

Space deployable structures are subjected to sudden heating when they move from ellipse, and during the deployment process the building unit will also undergo a large rotation and motion in addition to deformation. To analyze the impact of thermal loading on such structure with large motion and rotation, we proposed a beam model with coupled thermal effect in a framework of absolute nodal coordinate formulation. The coupled transient heat conduction equation and the structural dynamics equation are derived and solved iteratively. The proposed model is applied to examine the dynamics of a thin-walled tubular boom and a rotating flexible manipulator with thermal effect. It is shown that the thermal flutter can be well predicted with the coupled thermal–structural model and the thermal effect may have an important impact on dynamic response of the rotating flexible manipulator especially for low rotation speeds. The proposed model can be applied to study the influence of thermal effect on flexible multi-body dynamics.

## Acknowledgements

This work was supported by National Natural Science Foundation of China under Grants 10832002, 11290151 and 11221202.

## References

[1] M. Arnold, O. Brüls, Convergence of the generalized-$\alpha$ scheme for constrained mechanical systems, Multibody System Dynamics 18 (2007) 185–202.
[2] M. Berzeri, A.A. Shabana, Development of simple model for the elastic forces in the absolute nodal co-ordinate formulation, Journal of Sound and Vibration 235 (2000) 539–565.
[3] B.A. Boley, Approximate analyses of thermally induced vibrations of beams and plates, Journal of Applied Mechanics 39 (1972) 212–216.
[4] B.A. Boley, J.H. Weiner, Theory of Thermal Stresses, John Wiley and Sons, 1960.
[5] S. Erlicher, L. Bonaventura, O.S. Bursi, The analysis of the generalized-$\alpha$ method for non-linear dynamics problems, Computational Mechanics 28 (2002) 83–104.
[6] R.S. Foster, E.A. Thornton, An experimental investigation of thermally induced vibrations of spacecraft structures, in: Progress in Astronautics and Aeronautics, vol. 168, 1995, pp. 163–180.
[7] C.L. Foster, M.L. Tinker, G.S. Nurre, W.A. Till, The solar array-induced disturbance of the Hubble Space Telescope pointing system, NASA STI/Recon Technical Report N 95, 1995.
[8] D. Garcia-Vallejo, J. Mayo, J. Escalona, J. Dominguez, Efficient evaluation of the elastic forces and the Jacobian in the absolute nodal coordinate formulation, Nonlinear Dynamics 35 (2004) 313–329.
[9] D. Garcid, J. Valverde, J. Dominguez, An internal damping model for the absolute nodal coordinate formulation, Nonlinear Dynamics 42 (2005) 347–369.
[10] J. Gerstmayr, H. Irschik, On the correct representation of bending and axial deformation in the absolute nodal coordinate formulation with an elastic line approach, Journal of Sound and Vibration 318 (2008) 461–487.
[11] K.H. Hubner, E.A. Thornton, The Finite Element Method for Engineers, John Wiley and Sons, 1982.
[12] J.D. Johnston, E.A. Thornton, Thermal response of radiantly heated spinning spacecraft booms, Journal of Thermophysics and Heat Transfer 10 (1996) 60–68.
[13] J.D. Johnston, E.A. Thornton, Thermally induced attitude dynamics of a spacecraft with a flexible appendage, Journal of Guidance, Control, and Dynamics 21 (1998) 581–587.
[14] K.E. Ko, J.H. Kim, Thermally induced vibrations of spinning thin-walled composite beam, AIAA Journal 41 (2003) 296–303.
[15] C. Kong, H. Park, H. Lee, Study on comparison of atmospheric and vacuum environment of thermally-induced vibration using vacuum chamber, International Journal of Aeronautical and Space Sciences 11 (2010) 26–30.
[16] T. Li, Y. Wang, Deployment dynamic analysis of deployable antennas considering thermal effect, Aerospace Science and Technology 13 (2009) 210–215.
[17] T. Lida, J.N. Pelton, E. Ashford, Satellite Communications in the 21st Century: Trends and Technologies, Progress in Astronautics and Aeronautics, vol. 191, AIAA, Reston, Virginia, 2003.
[18] C. Liu, Q. Tian, H. Hu, Dynamics of a large scale rigid-flexible multibody system with composite laminated plates, Multibody System Dynamics 26 (2011) 283–305.
[19] A.A. Shabana, Definition of the slopes and the finite element absolute nodal coordinate formulation, Multibody System Dynamics 1 (1997) 339–348.

[20] A.A. Shabana, Dynamics of Multibody Systems, Cambridge University Press, 2005.
[21] E.A. Thornton, R.S. Foster, Dynamic response of rapidly heated space structures, Computational Nonlinear Mechanics in Aerospace Engineering 146 (1992) 451–477.
[22] E.A. Thornton, Y.A. Kim, Thermally induced bending vibrations of a flexible rolled-up solar array, Journal of Spacecraft and Rockets 30 (1993) 438–448.
[23] E.A. Thornton, G.P. Chini, D.W. Gulick, Thermal induced vibrations of a self-shadowed split-blanket solar array, Journal of Spacecraft and Rockets 32 (1995) 302–311.
[24] M.D. Xue, J. Duan, Z.H. Xiang, Thermally-induced bending–torsion coupling vibration of large scale space structures, Computational Mechanics 40 (2007) 707–723.
[25] Y.Y. Yu, Thermally induced vibration and flutter of a flexible boom, Journal of Spacecraft and Rockets 6 (1969) 902–910.